Structural and mechanical properties of Cr–Zr–N coatings with different Zr content

Linda Aissani[a,b], Mamoun Fellah[b,c], Corinne Nouveau [d], Mohammed Abdul Samad[e], Alex Montagne[f] and Alain Iost[f]

[a]Physics Department, ABBES Laghrour Khenchela University, Khenchela, Algeria; [b]Tribology, Materials Surface and Interfaces Group, Laboratory of Foundry, Annaba University, Annaba, Algeria; [c]Mechanical Engineering Departments, ABBES Laghrour Khenchela University, Khenchela, Algeria; [d]Mechanical Engineering Department, King Fahd University of Petroleum & Minerals, La.Bo.Ma.P, ENSAM, Rue Porte de Paris, Cluny, France; [e]Mechanical Engineering Department, King Fahd University of Petroleum & Minerals, Dhahran, Kingdom of Saudi Arabia; [f]Mechanical Surfaces and materials processing laboratory, ENSAM Arts et métiers Paris Tech, 8 Boulevard Louis XIV, Lille, France

ABSTRACT
Cr–Zr–N films have been synthesised using R.F reactive magnetron sputtering system on Si (100) wafer and XC100 steel substrate without heating. The structural, mechanical and friction coefficient evolution as a function of the Zr content were investigated by XRD, (EDS, WDS), WPS, XPS, SEM, AFM, nanoindentation, Scratch adhesion and pin-on-disc sliding wear tests. The results show, that, with increasing Zr content, the film structure changed with the coexistence of (Cr–N, Zr–N) crystallographic orientation mixture. The films formed a (Cr, Zr) N solid solution where Zr atoms substitute Cr atoms. CrN lattice parameter increased from 4.17 to 4.32 Å with the crystallite size refinement. The mechanical parameters (H, σ, E, H/E and H^3/E^2) were significantly improved in comparison to binary films, especially at 29 at.-% Zr. The friction and wear behaviour of the Cr–Zr (29 at.-% Zr)–N coating also showed a significant improvement.

Introduction

CrN coatings deposited by physical vapour deposition have been widely investigated for their industrial significance [1,2], in many applications such as cutting tools, mechanical compounds and surface steels due to their excellent mechanical properties, better oxidation resistance and tribological behaviour [3,4]. But, these binary coatings are unable to meet the increasing demands from the industrial development technology. Hence different groups of elements such as Ti, V, Al, Mo, Ni, Zr and Si have been introduced as a third element into these CrN coatings in an attempt to enhance their properties [4–8]. For example, Feng et al. [4] found that by adding Ti to the CrN coatings which were deposited on the Ti_6Al_4V alloy, improved the mechanical properties of CrN phase doped with 24.6 at.-% Ti. Yu et al. [9] examined the tribological behaviour of Cr–Al–N coatings, and found that the wear resistance of the Cr–Al–N films greatly improved as compared to the uncoated H13 steel substrate at 600°C. Also, the effect of addition of Ni on microstructure, mechanical properties and tribological behaviour of the binary CrN coating, have been reported by Kim et al. [10] and attributed this to, the formation of Cr–Ni–N solid solutions and the realisation of Cr–N bond energy of Cr_2N phase at 576.1 eV in parallel with Ni–Ni binding energy at

853.0 eV. They, also concluded that the hardness increased to more than 32.6 GPa with a small amount of Ni (2.7 at.-%) to CrN-based coatings and the highest wear resistance was obtained by the precipitation of the nanocrystalline phases at the CrN grain boundaries.

Some studies have reported that one of the most promising candidates to be added is zirconium that would form a ternary Cr–Zr–N system [3,11]. It has been reported that CrN coatings showed significant improvement in the hardness from 16.9 to 24.1 GPa with increasing Zr content from 0 to 2.3 at.-% [11]. Cr–Zr–N coatings have been prepared by DC reactive closed field unbalanced magnetron sputtering and their structure and surface morphology investigated [12]. The results indicated the formation of (Cr, Zr) N solid solution with microstructure evolution corresponding to the grain refinement. Kim et al. [3] have prepared the Cr–Zr–N films and examined the effect of Zr on the mechanical and wear properties. They found a significant improvement in the hardness, wear resistance and friction coefficient in comparison to the CrN coating.

However, these studies have been performed to investigate the general properties of Cr–Zr–N system, especially for the Zr content influence on the mechanical properties and wear behaviour. Only a few papers investigating the correlation between these properties

have been published [3,11]. According to our review of the previous studies [13–16], we found that H, E, σ, H/E and H^3/E^2 ratios are directly affected by the structure and composition of ternary films, and the consideration of these parameters are more important to evaluate the coating's mechanical and tribological behaviour. Hence, it has been observed that there is still a need to investigate and understand the relationship between the bonding configuration, constituent phases, the structural parameters and the mechanical and wear properties of the CrN coatings alloyed with Zr.

To address the above issues, the correlation between the bonding configurations, the constituent phases, the structural parameters (lattice parameters (a), crystallite size (L)), mechanical properties (Hardness (H), Young modulus (E), residual stress (σ), plasticity index (H/E) and plastic deformation resistance (H^3/E^2)) and tribological behaviour (friction coefficient (μ), adhesive and cohesive load failure $Lc_{1,2}$) of Cr–Zr–N system were comparatively investigated with pure CrN and ZrN coatings in this paper.

Materials and methods

CrN, ZrN and Cr–Zr–N thin films have been deposited at a total working pressure (Ar + N_2) of 0.4 Pa using R.F. magnetron sputtering system (NORDIKO type 3500, 13.56 MHz, 1.25 kW). Two separate target discs Cr (99.99%) and Zr (99.99%), with 10.16 cm of diameter each, were used as a substrate at 80 mm target distance and with an angle of +45° (Cr) and −45° (Zr) from the normal for all depositions, to obtain films with uniform thickness. The films were deposited onto Si (100) wafers and XC100[7] steel substrates. The details of the deposition conditions used in this work have been reported earlier [1]. The substrates were ground and polished to a surface roughness (Ra) of approximately 0.03 µm followed by ultrasonic cleaning for 5 min before being dried. Prior to deposition, the process chamber was evacuated to a vacuum of 2×10^{-5} Pa. The substrates were etched under Ar^+ ions bombardment for 5 min at −700 V (350 W) and 0.1 Pa. The targets were also cleaned under an Ar^+ discharge for 5 min, at −500 V (250 W) and 0.1 Pa. Just before starting deposition, CrN or/and (ZrN) coating was deposited by fixing the target voltage's Cr (Zr) at −900 V (630 W), with N_2/Ar ratio of 0.1 : 0.3 (N_2 :

0.1 Pa, Ar:0.3 Pa) for 5 min to increase the film adhesion. Cr–Zr–N films were deposited by adjusting voltage (power) of Cr and Zr targets from 0 to −900 V (0 to 650 W) and using a constant working pressure at 0.4 Pa during 90 min with the same ratio of Ar and N_2 flow rates (0.3:0.1). The deposition conditions are shown in Table 1.

The structure, lattice parameter (Bragg's equation) and crystallite size (Scherer's equation [7]) of the coatings were investigated by X-ray diffractometer (XRD, SIEMENS, D500) using $Co_{K\alpha}$ radiation operated at 45 kV. The thickness, surface morphology and fracture cross-sections of the coatings were investigated by scanning electron microscopy (SEM, JEOL JSM-5900LV). Microanalysis X (Oxford INCA x-act) was used to determine the elemental compositions. The chemical bonds of the coatings were determined using XPS (Riber SIA 100; AlKα, 1486.7 eV) at a pressure of 4×10^{-8} Pa after removing the contaminants from the surface of the coatings by sputtering with Ar^+ at 250 eV for 3 min at room temperature. The binding energy error was about 5%; the spectra were deconvoluted into multiple peaks with Gaussian line shapes by a multi-peaks fitting method. The coating surface roughness was examined by an atomic force microscope (AFM 100, APE research), which was operated in contact mode with the scan range of 3×3 µm.

Hardness and Young modulus were measured by means of a nanoindentation tester (MTS XP nano-indenter). A continuous stiffness measurement mode and tip oscillating with 45 Hz frequency and 2 nm for amplitude were used. A diamond Berkovich indenter with a tip radius of about 160 nm was used in the experiment, which was always less than 10% of the coating thickness, to ensure the hardness was not influenced by the substrate. The loading and unloading phases of the 10 indentations on each sample were carried out under load control with 10 mN maximum load at a nominal rate of 0.05 mN s^{-1}. The compressive residual stresses (σ) of the films were calculated using Stoney's equation (Newton's rings) [7].

The evolution of friction coefficient as a function of Zr at.-% content was evaluated using a pin-on-disc oscillating (TRIBO tester) at room temperature (23.5°C) with a relative humidity of 38.2.-%. A100Cr6 ball (6 mm diameter and 700 $HV_{0.2}$ hardness), was used as counter face under a constant normal load of 5 N and a

Table 1. Voltage (V), applied power (P) and chemical composition (at.-%) of the CrN, Cr–Zr–N and ZrN films deposited at 0.4 Pa during 90 min.

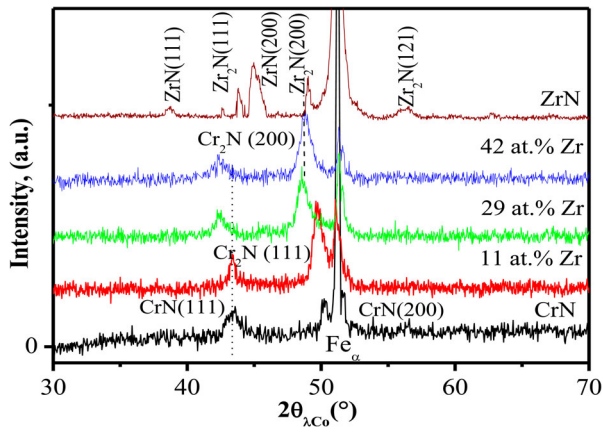| Film	Cr		Zr		Chemical composition (at.-%)					
	P (W)	V (V)	P (W)	V (V)	N	Cr	Zr	O	N/Cr + Zr)	Zr/Cr
CrN	650	900	…	…	47.8	50.0	…	2.2	0.96	0
$Cr_{0.40}$ $Zr_{0.11}N_{0.47}$	650	900	310	500	47.4	39.6	11.0	2.0	0.94	0.28
$Cr_{0.21}$ $Zr_{0.29}N_{0.47}$	650	900	630	900	47.3	21.3	28.8	2.6	0.95	1.34
$Cr_{0.10}$ $Zr_{0.42}N_{0.47}$	350	500	630	900	46.4	9.7	41.6	2.3	0.94	4.26
ZrN	…	…	630	900	47.4	…	48.8	3.8	0.97	…

Figure 1. The XRD pattern of Cr–Zr–N coating with different Zr content.

sliding speed of 0.5 mm s^{-1}. The friction coefficient was determined after 3 m sliding distance. The film adhesion was evaluated by means of scratch-tests (Scratch Tester Millennium 200), which were carried out using a Rockwell diamond indenter (diameter, radius, and conical angle of 0.2 mm, 200 μm and 120°, respectively). The stripping speed and length were 10 mm min^{-1} and 10 mm, respectively. After the wear tests, SEM and microanalysis X were used to evaluate the scratch scars and the worn surface morphology.

Results and discussion

Structural characterisation

The total content (100%) of (Cr, Zr, N and O) on the films deposited by various Zr (Cr) power targets are shown in Table 1. The N/Cr atomic ratio and thickness for CrN coating were found to be 0.96 and 1.26 μm, respectively, which are similar to the results reported in earlier studies [1,2,7,13].

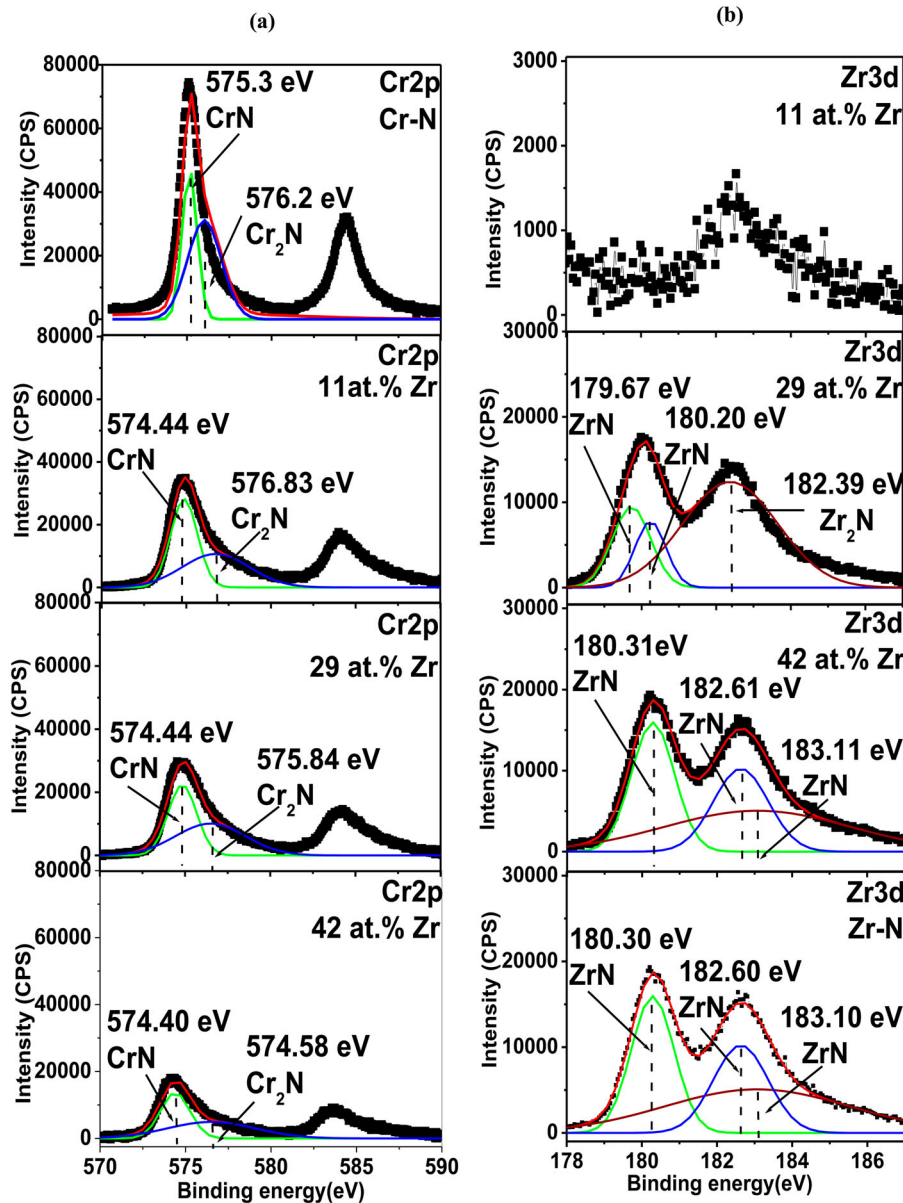The ZrN coating showed a N/Zr atomic ratio of around 0.97 and a film thickness of 1.28 μm. For

Figure 2. XPS spectra for Cr–Zr–N coatings with different Zr content: (a) Cr2p, (b) Zr3d, and (c) N1s.
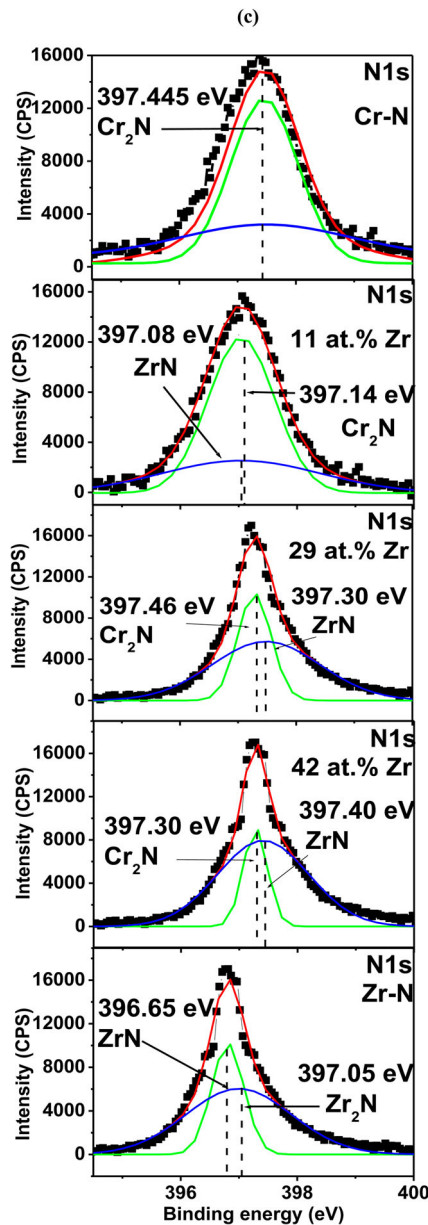
(c)

Figure 2. Continued.

Cr–Zr–N coatings, we found that if the Zr target's power increased from 260 to 630 W, the Zr content in the coatings increased gradually from 11 to 42 at.-%, whereas the Cr content decreased from 39.0 to 10 at.-%. These results reveal that the N content slightly decreased with increasing Zr, which led to an understoichiometric case of Cr–Zr–N coatings (N/(Cr+Zr)∼0.94) and an increase in Zr/Cr ratio from 0 to 4.26 with increasing the applied power of Zr target. The oxygen contamination in all the coatings was found to be very low in the range of 2–3.8 at.-%, which is interstitially induced in the films [3,10,14].

Figure 1 shows the XRD patterns of the Cr–Zr–N coating with varying Zr content, deposited onto XC100 steel substrates. The diffraction pattern of CrN coating presents two planes (111) and (200) at 43.49° and 51.67° corresponding to the fcc-CrN phase (JCPDF card, No. 01-0065). Another plane

(111) was observed at 50.27° corresponding to the hcp-Cr_2N phase (JCPDF card, No. 35-0803), which can be assigned to the formation of CrN and Cr_2N mixture [1,7]. The XRD patterns of ZrN films showed that the films were composed of well crystallised fcc-ZrN (200) plane at 45° with minor peaks of (111) ZrN at 38.9° (JCPDS card, No. 02-0956) and peaks of (111), (200) and (121) corresponding to Zr_2N (JCPDS card, No. 46-1204) at 43.86°, 49.05° and 56.25°, respectively [15]. The remarkable shifting of the CrN and ZrN diffraction peaks for (Figure 1) indicates an increase in lattice constants ($a_{CrN} = 4.170$ Å, $a_{ZrN} = 4.66$ Å), when compared with CrN and ZrN JCPDS data with the incorporation of N in the interstitial positions and compressive residual films [7].

At 11 at.-% Zr, three peaks in the diffraction pattern of ternary Cr–Zr–N coatings are detected, and the mixture (CrN, Cr_2N) also exists. The XRD pattern revealed a strong peak (111) of the hexagonal Cr_2N phase at 49.68° and CrN (111) and (200) reflection at 43.27° and 45.10°, respectively. However no diffraction peaks for Zr compounds were observed because of their less content which is insufficient to be detected.

From XRD results of 29 and 42 at.-% of Zr; random orientations were detected with the appearance of different reflection peaks as follows: (111) orientation of CrN, (111) and (200) from Zr_2N at 48.78° with (200) signal of ZrN. On the other hand, it is observed that the (111) CrN peak intensity is considerably reduced with increasing Zr content in the Cr–Zr–N system, which suggests that the structure becomes random with increasing Zr concentration as compared to pure CrN film. Furthermore, the position of CrN peaks shifted towards the lower diffraction angles with increasing Zr content which is attributed to the change of coating composition and the formation of new solid solution [16]. This may be explained by the substitution of Zr atoms in the CrN crystal lattice to form Cr–Zr–N solid solution, leading to a change in the lattice constants (because Zr ions are of bigger size than Cr ions) [3] and also the induction of compressive stresses by increasing the ion bombardment energy (630 W) [3,7]. Similar behaviour was also observed in some other Cr–X–N films [7,17].

In order to obtain more information about the chemical bonds of Cr–Zr–N coatings with varying Zr content, XPS analysis was carried out for N1s, Cr2p, and Zr3d spectra (Figure 2).

As we can see for CrN film, N1s spectrum shows a single wide peak, which can be de-convoluted into two similar chemical binding energies at 397.4 eV and Cr2p peaks have been systematically decomposed into two bonds of intensities at 575.0 and 576.40 eV (Figure 2(a,c)), which are corresponding to Cr–N bonds [18] and suggest a mixture of Cr_2N (576.40 eV) and CrN (575.0 eV) [19].
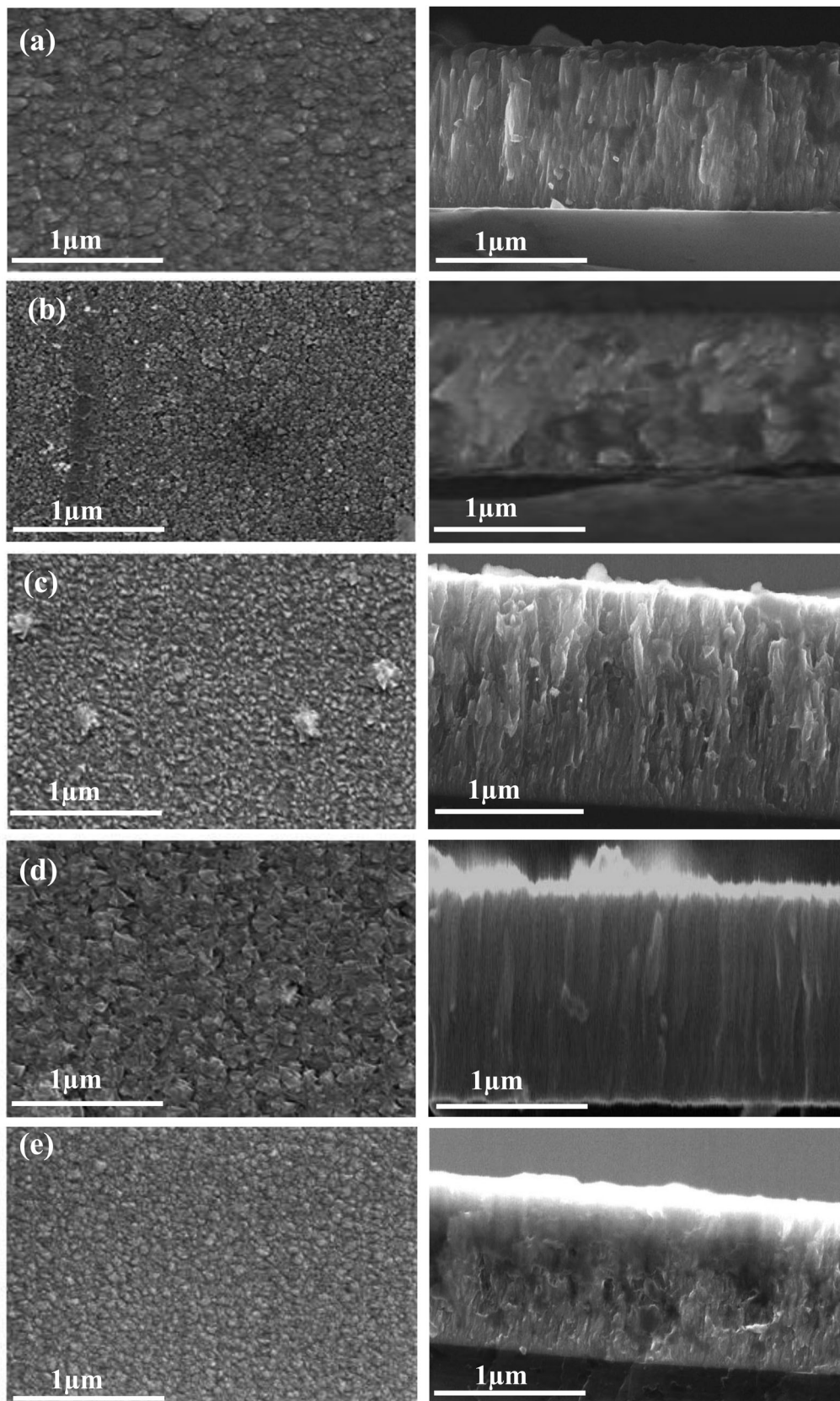
Figure 3. SEM cross sections and surface morphologies of: (a) CrN, (b) Cr–Zr (11 at.-% Zr)–N, (c) Cr–Zr (29 at.-% Zr)–N, (d) Cr–Zr (42 at.-% Zr)–N, and (e) ZrN films.

The Zr3d and N1s XPS spectra acquired from the ZrN film are shown in Figure 2(b,c). The Zr3d spectra can be de-convoluted into three peaks, where two peaks are compatible with ZrN from a doublet consisting of $Zr3d_{5/2}$ (179.50 eV) and $Zr3d_{3/2}$ (181.90 eV), while the third peak of $Zr3d_{1/2}$ (182.2 eV) for Zr_2N. The N1s spectra shown at 396.65 and 397.10 eV, can be assigned to Zr–N binding energy [3].
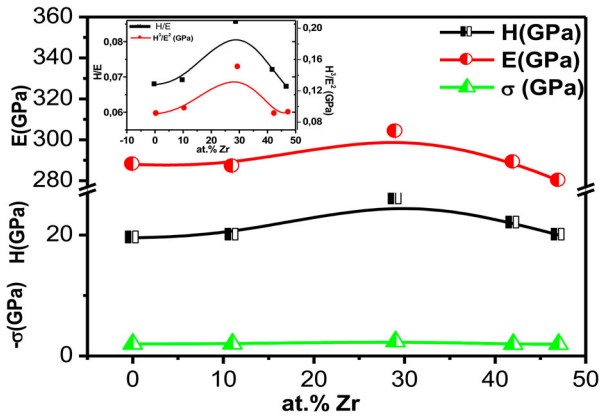
Figure 4. Hardness, Young's modulus, residual stress, *H/E* and *H*3/*E*2 ratios of Cr–Zr–N coatings with different Zr content.
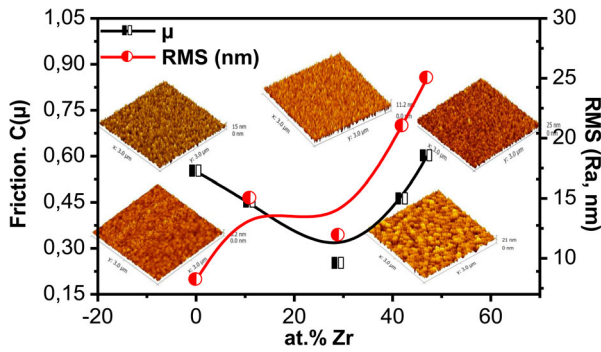

Figure 5. Friction coefficient, the average roughness (Ra) value, and the AFM images for Cr–Zr–N, coating with different Zr content.

For Cr–Zr–N coatings, the main peak of N1s spectra corresponds to Cr_2N (397.45 and 397.14 eV) and the minor peak corresponds to Zr_2N (397.1 and 397.4 eV) [20]. The N–Cr binding intensity decreases gradually, while N–Zr binding increases. This suggests that Cr_2N and Zr_2N coexist in the coatings and the content of Zr_2N increases while the Cr_2N content decreases with increasing Zr content. A negative shift from 574.80 and 575.68 eV for 11 and 29 at.-% Zr, down to 575.01 eV for 42 at.-% Zr, for the peaks of Cr2p is observed, suggesting a change in the Cr binding nature from a Cr–N [20] to a pure metallic Cr–Cr [18] by the gradual transformation of fcc-CrN to hcp-Cr_2N. Zr3d spectra is illustrated in Figure 2(b). Two main peaks for ZrN ($Zr3d_{5/2}$ (180.30 eV) and $Zr3d_{3/2}$ (182.60 eV)) with a large percentage of area and a minor peak corresponding to Zr_2N ($Zr3d_{3/2}$) at 183.10 eV [3], is also identified in the XRD patterns. The XRD and XPS analysis results reveal that Cr–Zr–N coatings are substitutional (Cr–N, Zr–N) mixture which exhibit a crystalline structure.

The SEM micrographs and cross-section of the coatings are displayed in Figure 3. For CrN coating (Figure 3(a)), there exhibits a dense columnar structure without micro-droplets or craters in the surface morphology. The crystallite size and the lattice parameter

of CrN coatings calculated from (111) plane at 43.49° angle were 18.3 nm and 4.17 Å, respectively. According to Mahieu's SZM [21] the film structure belongs to the zone I_c structure caused by the compressive state film. Similar morphology evolution has been reported in the literature [7,11,22], which is a result of the mutual interference of the intermediate fcc-CrN and hcp-Cr_2N.

With an increase in the Zr target power, ion bombardment with higher energetic elements leads to the compact columnar microstructure [12], which is between zone I_c and zone T [21]. The crystallite size of the Cr–Zr–N coatings clearly decreased from 20 nm at 11 at.-% Zr, which is close to CrN structure, to 10.8 nm at 29 at.-% Zr (Figure 3(b,c)), while the lattice parameter, increased from 4.17 Å (CrN) to 4.32 Å (29 at.-%), which causes more Zr ions to occupy the Cr sites and the ZrN re-nucleation through films deposition [11,16], than the structure becomes between zone I_a and zone I_b at 42 at.-% Zr (Figure 3(d)). The ZrN coating exhibited low thickness and rough surface as compared to CrN and Cr–Zr–N films. Also, it showed a compact columnar structure with a small crystallite size (19.6 nm) (Figure 3(e)), and a lattice parameter of 4.66 Å, which is slightly higher than that, obtained from ZrN JCPDS data (4.65 Å) due to the selective capture of interstitial nitrogen atoms during ZrN film deposition [14]. This structure is compatible with zone I_c [21,23].

The roughness analysis presented an acute vertices growth type for all coating surfaces (Figure 5). The surface roughness (Ra) value decreased from 15 to 11 nm at 11 and 29 at.-%, respectively, than increased to 21 nm at 42 at.-% Zr, which may be related to the formation of a new composite structure and the competitive growth between Cr–N and Zr–N [24,25].

Mechanical properties

The residual stress of Cr–Zr–N films as a function of Zr content is presented in Figure 4. As shown; all coatings are in compressive stress state. The incorporation of Zr into CrN coatings leads to the gradual increase in the residual stress from −1.89 to −2.04 GPa at 0 to 29 at.-% Zr. This may be attributed to the increase in the CrN lattice parameter [26].

Hardness and Young modulus of CrN and ZrN coatings are about $H_{CrN} = 19.53$ GPa, $E_{CrN} = 287.91$ GPa and H_{ZrN} 20.00 GPa, $E_{ZrN} = 270.00$ GPa, respectively [3,11]. In the case of Cr–Zr–N systems (11–29 at.-% Zr), with strong mixture of CrN and ZrN, the hardness and Young modulus increased, to reach the highest values of 26.00 and 304.00 GPa at 29 at.-% Zr which are attributed to the formation of a nanocomposite structure, crystallite size refinement, formation of strengthening solid solution and an increase in the residual stresses [11,16,27]. According
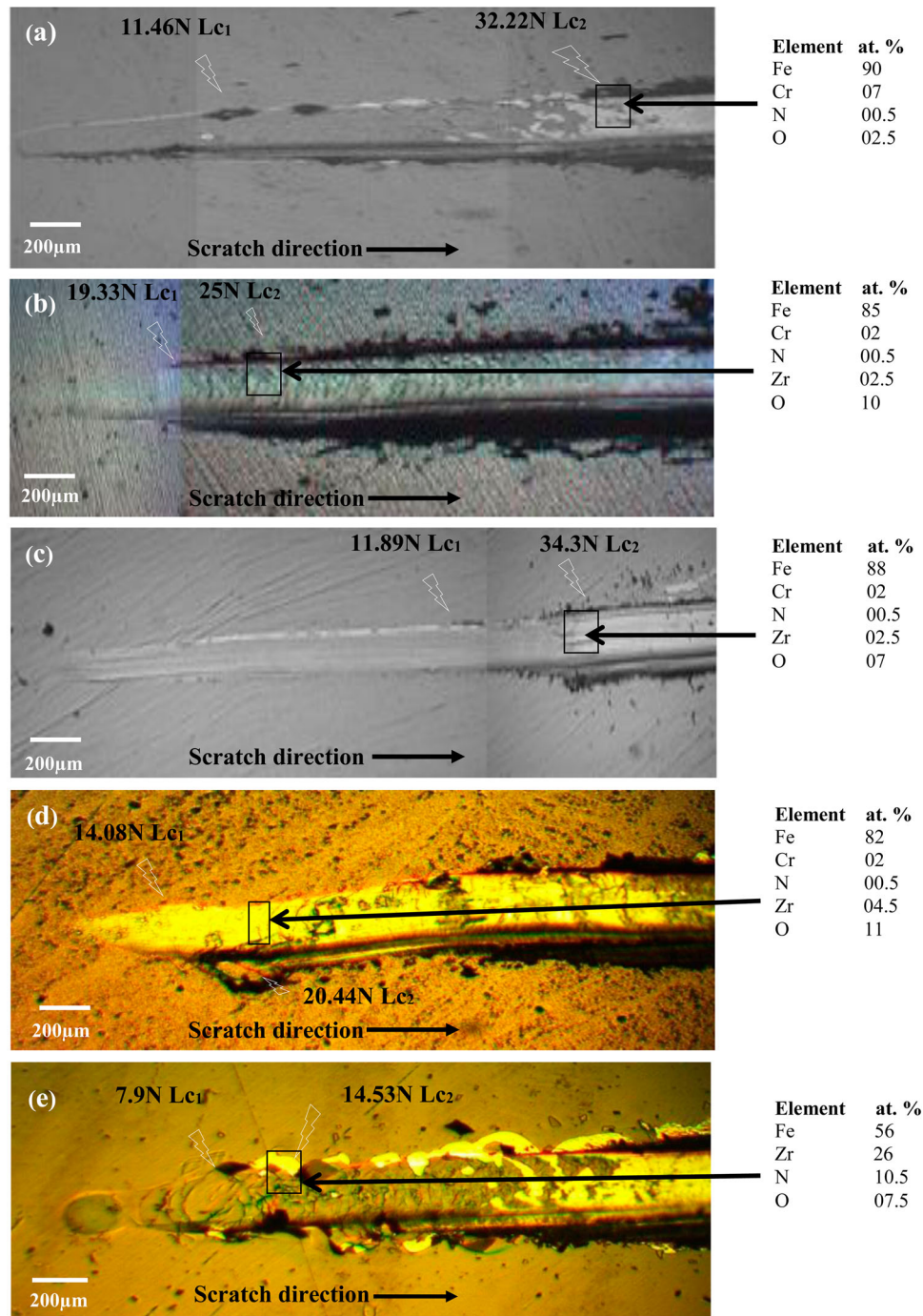
Figure 6. Scratch tracks micrographs of: (a) CrN, (b) Cr–Zr (11 at.-% Zr)–N, (c) Cr–Zr (29 at.-% Zr)–N, (d) Cr–Zr (42 at.-% Zr)–N, and (e) ZrN films.

to the XPS analysis, the peak shifting of Cr2p binding energy states suggests that the bonding character changed from Cr–N to Cr–Cr bonds due to the charge transfer from nitrogen to Cr atoms as a function of Zr content and the increase of Zr–N bonds where it's harder than Cr–N [11]. The decrease in hardness value (22 ± 0.10 GPa) at 42 at.-% Zr was not observed in previous studies [3,11], which may have been caused due to the formation of the rough surface and the random structure with an increase in the Zr content. Moreover, the Young modulus did not follow the opposite trend with higher values as reported earlier [3,11].

Many researchers have investigated the variation of H/E and H^3/E^2 ratios and obtained large information about the resistance against elastic and plastic deformation [16]. The H/E and H^3/E^2 ratios are about 0.0690, 0.0971 GPa and 0.0671, 0.0922 GPa for CrN and ZrN coatings, respectively (Figure 4). The substitution of Zr into Cr crystal lattice increases the H/E and H^3/E^2 to the maximum values of 0.0855, 0.1901 GPa at 29 at.-% Zr and then decreases slightly to 0.0619, 0.0904 GPa at 42 at.-% Zr. This suggests an improvement in the penetration resistance and elastic tensile strength under load [16,28], which are associated with a high hardness

and Young modulus of the films closest to the XC100 substrate.

Evolution of friction coefficient and scratch test

As shown in Figure 5, the mean friction coefficient values, showed a downward trend with an increase in the at.-% Zr content. As seen, the friction coefficient decreases slightly from 0.55 to 0.46 with a reduction in the content of Zr from 0 to 11 at.-%, and subsequently decreases rapidly to reach a lowest value of 0.25 at 29 at.-% Zr. After this stage, the variations in friction coefficient values becomes smaller and the friction coefficient slightly increases during the remaining at.-% Zr content to reach a high mean value of 0.52 at 48 at.-% Zr. This behaviour can be attributed to a polishing process resulting in an accidental structure in the coatings establishing a smooth wear track surface, by ploughing away the surface asperities and roughness irregularities [3,7].

Scratch test results are displayed in Figure 6. CrN coating showed a good adhesion and little damage of the film (Figure 6(a)). Very low concentration of Cr and N elements were observed. The cohesive and adhesive failure critical loads are in the range of $Lc_1 \approx 11.46$ and $Lc_2 \approx 32.22$ N, respectively. These values can be attributed to the high residual stress of the CrN film.

At 11 at.-% Zr (Figure 6(b)), in the initial stages of the scratches, smooth and adhesive wear without any sign of abrasive debris was observed and its wear rate was too negligible compared to CrN coatings, which was attributed to its low surface roughness and high hardness values [16]. However, at 29 at.-% of Zr (Figure 6(c)), an adhesive critical high load ($Lc_2 \approx 34.3$ N) and delamination fracture mechanism of coating from the substrate was observed at the edges of the scratches track. This was mainly due to the adhesive action of the wear debris [3,10,11].

At 42 at% Zr (Figure 6(d)), the adhesive action is significantly lower ($Lc_2 \approx 20.44$ N) than in the cases of 29 at.-% Zr; and only Fe of the substrate and O were detected in the scratches tracks. The results also show that the addition of 42 at.-% of Zr to system has deteriorated the adhesion proprieties of the coatings. This can be attributed to the reduction in the mechanical properties.

Finally, for ZrN film, a significant decrease of the Lc_1 was obtained, up to 7.9 N. The ZrN film revealed a lower adhesive critical load ($Lc_2 \approx 14.5$ N). Nevertheless, a brittle failure mode was observed, which was manifested by the formation of lateral cracks and chipping at the edges and the middle of the scratch tracks (Figure 6(e)). This can be attributed to the formation of the macro particles in the ZrN film, which act as stress raisers and cause the cracks to initiate [29,30].

Conclusion

The structure and mechanical proprieties of Cr–Zr–N coating have been investigated. The following conclusions can be drawn:

(i) The deposited Cr–Zr–N coatings showed a columnar compact structure with a mixture of fcc (CrN, ZrN) and hcp (Cr_2N, Zr_2N) phases with Cr_2N (111) preferential orientation.

(ii) The Cr–Zr–N crystallite size decreased and the lattice parameter increased as zirconium content increased from 0 to 29 at.-% with an improved surface roughness due to the crystallite size refinement.

(iii) The residual stress, hardness, Young's modulus, H^3/E^2 and H/E ratios of Cr–Zr–N coatings increase to reach high values of −2.04, 26, 304 GPa, 0.0855 and 0.1901 GPa, respectively, at 29 at.-% Zr and then decrease due to the formation of strengthening (Cr–N, Zr–N) mixture, preferred crystalline orientation and grain refinement.

(iv) Cr–Zr (29 at.-% Zr)–N film exhibited the lowest friction coefficient among all the films which were evaluated.

(v) The sliding performance of Cr–Zr (29 at.-% Zr)–N was extremely superior than CrN and ZrN.

ORCID

Corinne Nouveau   http://orcid.org/0000-0002-5552-2020

References

[1] Pradhan SK, Nouveau C, Vasin A, et al. Deposition of CrN coatings by PVD methods for mechanical application. Surf Coat Technol. 2005;200:141–145.

[2] Shah HN, Jayaganthan R, Kaur D. Effect of sputtering pressure and temperature on DC magnetron sputtered CrN films. Surf Eng. 2010;26(8):629–637.

[3] Kim GS, Kim BS, Lee SY, et al. Structure and mechanical properties of Cr–Zr–N films synthesized by closed

field unbalanced magnetron sputtering with vertical magnetron sources. Surf Coat Technol. 2005;200:1669–1675.

[4] Feng X, Zhou H, Wan Z, et al. Effect of Ti content on structure and mechanical properties of Cr–Ti–N films. Surf Eng. 2017;33(8):619–625. DOI:10.1080/02670844.2016.1212531

[5] Fallqvist M, Olsson M. The influence of surface defects on the mechanical and tribological properties of VN-based arc-evaporated coatings. Wear. 2013;297:1111–1119.

[6] Kim HK, La JH, Kim KS, et al. The effects of the H/E ratio of various Cr-N interlayers on the adhesion strength of Cr-Zr-N coatings on tungsten carbide substrates. Surf Coat Technol. 2015;284:230.

[7] Aissani L, Nouveau C, Walock MJ, et al. Influence of vanadium on structure, mechanical and tribological properties of CrN coatings. Surf Eng. 2015;31(10):779–788.

[8] Twu MJ, Hu CC, Liu DW, et al. Effects of TiN, CrN and TiAlN coatings using reactive sputtering on the fatigue behavior of AA2024 and medium carbon steel specimens. J Exp Nanosci. 2016;11(7):581–592.

[9] Yu CY, Wang SB, Li TB, et al. Tribological behavior of CrAlN coatings at 600°C. Surf Eng. 2013;29(4):318–321.

[10] Kim DH, Zhang TF, Shin JH, et al. Microstructure and mechanical properties of Cr–Ni–N coatings deposited by HiPIMS. Surf Eng. 2016;32(4):314–320.

[11] Aouadi SM, Maeruf T, Twesten RD, et al. Physical and mechanical properties of chromium zirconium nitride thin films. Surf Coat Technol. 2006;200:3411–3417.

[12] Chantharangsi C, Denchitcharoen S, Chaiyakun S, et al. Structure and surface morphology of Cr-Zr-N thin films deposited by reactive DC magnetron sputtering. Procedia Eng. 2012;32:868–874.

[13] Hones P, Sanjines R, Lévy F. Characterization of sputter-deposited chromium nitride thin films for hard coatings. Surf Coat Technol. 1997;91(95):398–402.

[14] Ju H, Xu J. Microstructure, oxidation resistance, mechanical and tribological properties of Ti-Y-N films by reactive magnetron sputtering. Surf Coat Technol. 2015;283:311–317.

[15] Pelleg J, Zevin LZ, Lungo S, et al. Reactive-sputter-deposited TiN films on glass substrates. Thin Solid Films. 1991;197:117–129.

[16] Zhao H, Ni Z, Ye F, et al. The structure and mechanical properties of magnetron sputtered VSiN coatings. Surf Eng. 2017;33(8):585–591. DOI:10.1080/02670844.2016.1139027

[17] Hones P, Sanjines R, Lévy F. Sputter deposited chromium nitride based ternary compounds for hard coatings. Thin Solid Films. 1998;332:240–246.

[18] Conde A, Cristóbal AB, Fuentes G, et al. Surface analysis of electrochemically stripped CrN coatings. Surf Coat Technol. 2006;201:3588–3595.

[19] Seok JW, Jadeed NM, Lin RY. Sputter-deposited nanocrystalline Cr and CrN coatings on steels. Surf Coat Technol. 2001;138(1):14–22.

[20] Bertoti I. Characterization of nitride coatings by XPS. Surf Coat Technol. 2002;151–152:194–203.

[21] Mahieu S, Ghekiere P, Depla D, et al. Biaxial alignment in sputter deposited thin films. Thin Solid Films. 2006;515:1229–1249.

[22] Tański T, Lukaszkowicz K. Structure and properties of PVD coatings deposited on aluminum alloys. Surf Eng. 2012;28(8):598–604.

[23] Lamni R, Sanjinés R, Wojtan MP, et al. Microstructure and nanohardness properties of Zr-Al-N and Zr-Cr-N thin films. J Vac Sci Technol A. 2005;23(4):593–598.

[24] Bhatti J, Fazal MA, Khan AF, et al. Investigation of the mechanical properties of electrodeposited nickel and magnetron sputtered chromium nitride coatings deposited on mild steel substrate. J Adhes Sci Technol. 2016;30(20):2224–2235.

[25] Khlifi K, Ben Cheikh Larbi A. Investigation of adhesion of PVD coatings using various approaches. Surf Eng. 2013;29(7):555–560.

[26] Ye F, Zhao L, Mu C, et al. Influence of yttrium addition on reactive sputtered W–Y–N coatings. Surf Eng. 2017;33(8):626–632. DOI:10.1080/02670844.2016.1231758

[27] Xu J, Ju H, Yu L. Microstructure, oxidation resistance, mechanical and tribological properties of Mo-Al-N films by reactive magnetron sputtering. Vacuum. 2014;103:21–27.

[28] Zhao H, Ye F. Effect of Si-incorporation on the structure, mechanical, tribological and corrosion properties of WSiN coatings. Appl Surf Sci. 2015;356:958.

[29] Tung HM, Huang JH, Tsai DG, et al. Hardness and residual stress in nanocrystalline ZrN films: effect of bias voltage and heat treatment. Mater Sci Eng A. 2009;500(1):104–108.

[30] Gruss KA, Davis RF. Adhesion measurement of zirconium nitride and amorphous silicon carbide coatings to nickel and titanium alloys. Surf Coat Technol 1999;114:156–168.